JOURNAL OF THERMOPHYSICS AND HEAT TRANSFER
Vol. 16, No. 4, October–December 2002

Experimental Study of Evaporative Heat Transfer in Sintered Copper Bidispersed Wick Structures

X. L. Cao,* P. Cheng,† and T. S. Zhao‡
Hong Kong University of Science and Technology, Hong Kong, People's Republic of China

An experiment has been carried out on evaporative heat transfer in rectangular bidispersed wick structures heated by a grooved block from the top. Three bidispersed wick structures, having large/small pore-diameter ratios of 200/80, 400/80, and 800/80 μm, were formed by sintering copper powder. For comparison, two monodispersed wick structures having pore diameters of 80 and 800 μm, respectively, were also tested. It was found that the heat transfer coefficient and the critical heat flux of a bidispersed wick are much higher than that of a monodispersed wick having its pore diameter equal to the smaller pore diameter of the bidispersed wick. It is also found that for bidispersed wicks with the same small-pore diameter there exists an optimal large-pore diameter that gives both the highest heat transfer coefficient and the highest critical heat flux. Finally, the effect of the adverse hydrostatic head on the heat transfer performance in the wick is shown.

Nomenclature

A_h	=	heating surface area, m^2
a	=	length of heating block, m
h	=	heat transfer coefficient, W/m^2 K
K	=	permeability, m^2
$\dot{m}$	=	mass flow rate, kg/m^2 s
Q	=	heat power, W
T_l	=	temperature of the subcooled liquid water, °C
T_s	=	saturation temperature, °C
T_v	=	temperature of the exhaust vapor, °C
T_W	=	temperature of the heating block, °C
ΔH	=	adverse hydrostatic head, mm
ε	=	porosity

Subscripts

l	=	liquid
s	=	saturation
v	=	vapor
w	=	wall

Introduction

A CAPILLARY pumped loop (CPL) is a two-phase heat transfer device capable of transporting a large heat load over a long distance, with a small temperature difference across the system. The CPL is now the baseline design for thermal control of the Earth Observing System (EOS-AM), Mars Surveyor Program, and Hubble Space Telescope. It is also a prime candidate for thermal control in several future spacecraft.[1,2] Much research in the past has been conducted to improve the performance and reliability of CPL systems, including component design modification and upgrades, as well as system performance enhancements.

The capillary evaporator, being a key component of a CPL, has been modified progressively, and the heat and mass transfer processes in its wick have been investigated extensively. For example, Deng et al.[3] investigated experimentally the heat transfer coefficient and the critical heat flux of inverted meniscus evaporators consisting of steel screens with various mesh sizes. Cao and Faghri[4,5] investigated both analytically and numerically the flow and heat transfer in a porous structure with partial heating and evaporation on the upper surface. Khrustalev and Faghri[6] investigated heat and mass transfer processes around a heated triangular solid fin penetrating into a wetted porous structure. More recently, Liao and Zhao[7] investigated experimentally capillary-driven heat and mass transfer processes in a vertical rectangular capillary porous structure of glass beads with a grooved heating boundary at the top. The experimental results showed that with an increase of the imposed heat flux, the heat transfer coefficient increases to a maximum value and then decreases afterward. In another paper, Zhao and Liao[8] analyzed heat and mass transfer in such a capillary porous structure by simultaneously solving the problem of evaporating capillary meniscus at the pore level and the problem of fluid flow through a porous medium. The results based on their model agreed well with their experimental data. Subsequently, Liao and Zhao[9] visually studied the phase-change heat transfer in a two-dimensional porous structure with a partial-heating boundary. Their results revealed that for a small or moderate heat flux, isolated bubbles formed, grew, and collapsed beneath the heating fins in a cyclic manner with a nearly constant frequency. When the heat flux was sufficiently high, a vapor film would form beneath the heating fin and the critical heat flux would occur.

The wick structures used in the aforementioned investigations are all monodispersed porous media that provide only a modest amount of heat transfer capacity. To develop evaporators capable of withstanding high heat fluxes, the bidispersed wick structure, which is characterized by two capillary radii (one large and one small), has been used in heat pipes and looped heat pipes (LHPs).[10,11] This type of wick will also have promising applications in the evaporator of CPLs.[12,13] However, few investigations have been carried out on heat and mass transfer in a bidispersed wick. North et al.[14] studied the liquid film evaporation from bidispersed capillary wicks in heat pipe evaporators and found that a nearly constant wall-to-vapor temperature difference is present over a large range of input heat fluxes because of the formation of a high-density evaporating thin film within this wick. Most recently, Chen et al.[15] investigated two-phase flow and flow boiling heat transfer in a bidispersed porous channel. They found that the permeability of the bidispersed porous medium was almost the same as the monodispersed porous medium when the macropore diameter of the bidispersed medium was the same as the pore diameter of the monodispersed medium. They also found that the flow boiling heat transfer coefficient of bidispersed porous media was higher than that of monodispersed media at high

Received 14 August 2001; revision received 12 June 2002; accepted for publication 17 June 2002.

*Research Assistant, Department of Mechanical Engineering, Clear Water Bay, Kowloon.
†Professor, Department of Mechanical Engineering, Clear Water Bay, Kowloon. Associate Fellow AIAA.
‡Associate Professor, Department of Mechanical Engineering, Clear Water Bay, Kowloon.

heat flux when the pore diameter of monodispersed porous media was the same as the macropore diameter of the bidispersed media.

In this paper, experiments were carried out to study capillary-driven heat and mass transfer processes in bidispersed porous structures saturated with water, which were subjected to a grooved heating boundary from the top. For comparison, two monodispersed porous wicks were also tested under the same conditions. As shown in the experimental setup in Fig. 1, the capillary force generated at the interface between the heated fin and the wick structure is balanced by the flow drag through the porous wick and the adverse hydrostatic head. The effects of this adverse hydrostatic heads on the porous samples are investigated.

Experimental Apparatus and Procedures

Figure 1 shows the experimental apparatus used in the present investigation. It consisted of two major parts: the liquid supply system and the test section. The liquid supply system consisted of a water tank, a water-level controller, and an overflow container. The deionized water draining from the water tank was bifurcated into two streams in the water-level controller: one stream directed toward the test section, the other directed toward the overflow container. Thus, the water level in the water-level controller could be kept constant during the experiments. The adverse hydrostatic head ΔH (the height difference between the top of the porous structure and the water level) was controlled by the elevation of the platform lifter, on which the water-level controller was placed.

The test section is illustrated at the left portion of Fig. 1. The test sample was fixed in the middle of a Teflon® sheath, which was placed in the upper portion of an aluminum container. A stainless film (0.1 mm in thickness) serving as a heater, a mica sheet serving as an electrical insulator, and a Teflon cover serving as a heat insulator were mounted on the top of the test sample. The lower portion of the aluminum container served as a water pool, into which water was directed from the water-level controller. Because of the capillary force generated at the liquid/vapor interface near the heated surface, the subcooled liquid flowed upward from the bottom by overcoming the gravity and the drag force in the porous medium. The inlet temperature of the water was well controlled by a resistance temperature detector (RTD) temperature controller with a 100-W heater located in the lower portion of the water pool. The space between the aluminum container and the Pyrex® case was filled with glass fiber wool for thermal insulation.

As shown in Fig. 2, the tested wick samples were formed by sintering copper powder and bonded to a grooved copper block. Three bidispersed wicks having large/small pore diameter ratios of 200/80, 400/80, and 800/80 μm, respectively, as well as two monodispersed wicks having pore diameters of 80 and 800 μm, respectively, were tested. The geometric factors of the five porous samples are listed in Table 1, and their dimensions are shown in Fig. 2. Other properties, including porosity and permeability of the tested samples obtained by Chen et al.,[15] are also listed in Table 1.

Seven T-type thermocouples were used to measure temperatures, one inserted into the middle of the water pool, two beneath of the wick, two inserted into the middle of the copper block, and the other two at the outlet of the vapor. The bulk water temperature was kept at 95°C during all of the experiments. It usually took about 0.5–1 h for the system to be stabilized. All experimental data were collected under steady-state conditions. The physical quantities measured during the experiments included the temperatures of the heating block T_W, the subcooled liquid water T_l, and the exhausted vapor T_v; the mass flow rate of water m; as well as the imposed heating load Q. All of the temperatures were recorded by a data acquisition system (IMP3595, Solartron). The mass flow rate of water was measured by reading the change per unit time of the total mass of the water tank and the overflow container. The imposed heating load was obtained by measuring the power supply to the film heater with a power meter.

In the present study, h is defined as

$$h = Q/A_h(T_W - T_s) \tag{1}$$

where A_h can be described as the cross-sectional area of the copper block (equal to 9 cm^2 in this experiment). T_W is the mean temperature

Table 1 Properties of the wick samples

	Sample				
Parameter	1	2	3	4	5
Large-pore diameter, μm	80	800	200	400	800
Small-pore diameter, μm	80	800	80	80	80
Porosity ε, %	46	49	52	54	57
Permeability K, $\times 10^{10}$ m^2	0.267	6.035	2.235	3.078	5.642

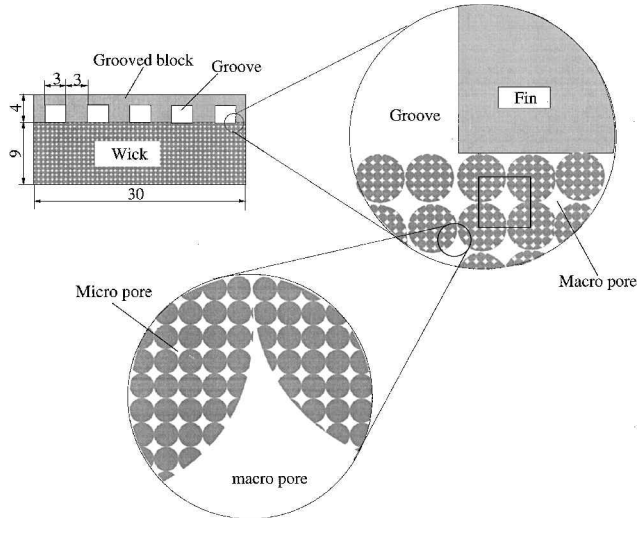

Fig. 2 Schematic of the bidispersed test sample (dimensions in millimeters).

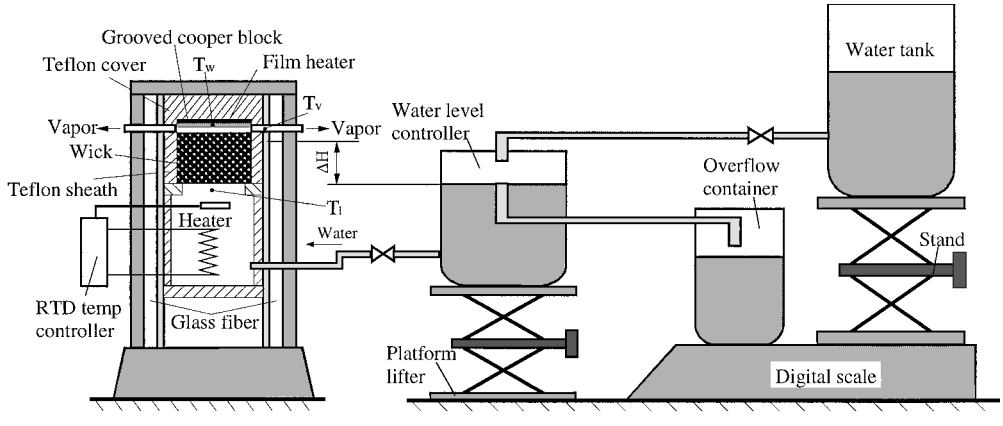

Fig. 1 Schematic of the experimental apparatus.

of the heating block, which was obtained by averaging the readings of the two thermocouples inserted into the middle of the copper block. T_s is the saturation temperature of water, which was obtained approximately by averaging the readings of the two thermocouples located at the outlet of vapor. Note that the temperature across the copper block was rather uniform, reflected by the temperature difference between the two measuring points being less than 0.1°C. The thermocouples were calibrated to ensure the accuracy within ±0.2°C. By the use of the uncertainty estimation method of Kline and McClintock,[16] it was estimated that the uncertainty in the heat transfer coefficient was within 6.1%.

Results and Discussion

Figures 3 and 4 show the wall temperature variation and the heat transfer coefficient vs the imposed heat flux for all five porous samples under the adverse hydrostatic head of $\Delta H = 4.0$ mm. As shown in Fig. 3, the wall temperature increases with increasing heat flux. Moreover, at a given heat flux, the wall temperature is the highest for sample 1 (monodispersed medium with a pore diameters of 80 μm) and the lowest for sample 4 (bidispersed medium with a pore diameter ratio of 400/80 μm. The reason for such a behavior will be explained later in this paper.

Figure 4 shows that the heat transfer coefficients of all of the tested porous samples gradually increased, reached a peak value, and dropped off thereafter, as the imposed heat flux was increased. The end of each curve represents the critical heat flux corresponding to each tested sample. Consider first the heat transfer performance of the two monodispersed wicks, sample 1 (with a pore diameter of 80 μm) and sample 2 (with a pore diameter of 800 μm). As can be seen from Fig. 4, both the heat transfer coefficient and the critical heat flux of the monodispersed wick increased significantly as the pore diameter was increased from 80 to 800 μm. For the problem under consideration, the subcooled liquid was pumped upward to the heated surface by the capillary force that overcame the flow drag through the wick and the adverse hydrostatic head. Although the capillary force for the small-pore-diameter wick (sample 1) was larger than that for the large-pore-diameter wick (sample 2), the corresponding flow drag force was increased with the decrease of the pore diameter, resulting from the lower permeability, as is evident from Table 1. The increase of the flow resistance caused a reduction in the mass flow rate of the subcooled liquid. Consequently, only a small amount of liquid could be provided to the interface of the heated surface. It follows that a smaller-pore-diameter wick leads to a reduction in both the heat transfer coefficient and the critical heat flux. For this reason, the wall temperature of sample 1 (having a pore diameter of 80 μm) is higher than that of sample 2 (having a pore diameter of 800 μm) at the same imposed heat flux, as shown in Fig. 3.

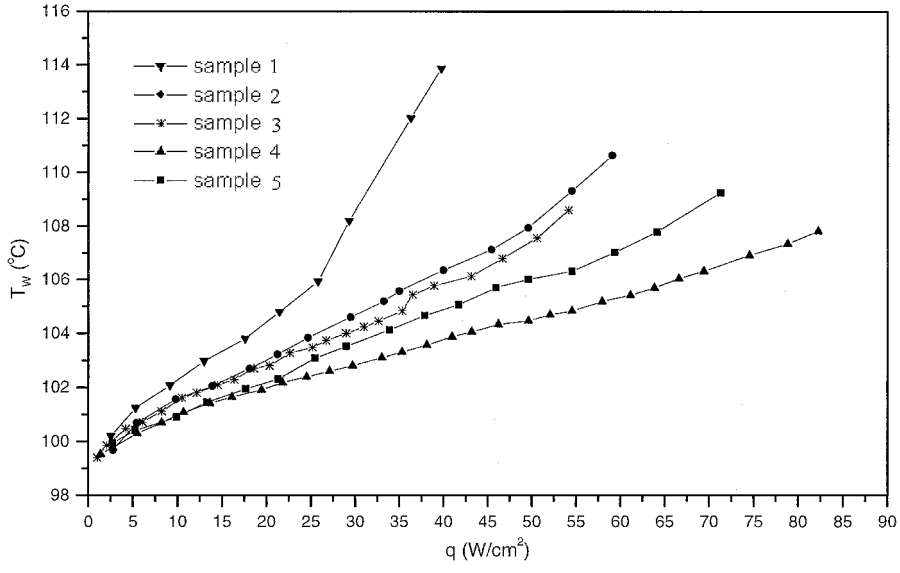

Fig. 3 Mean temperature of the heating block vs imposed heat flux at $\Delta H = 4.0$ mm.

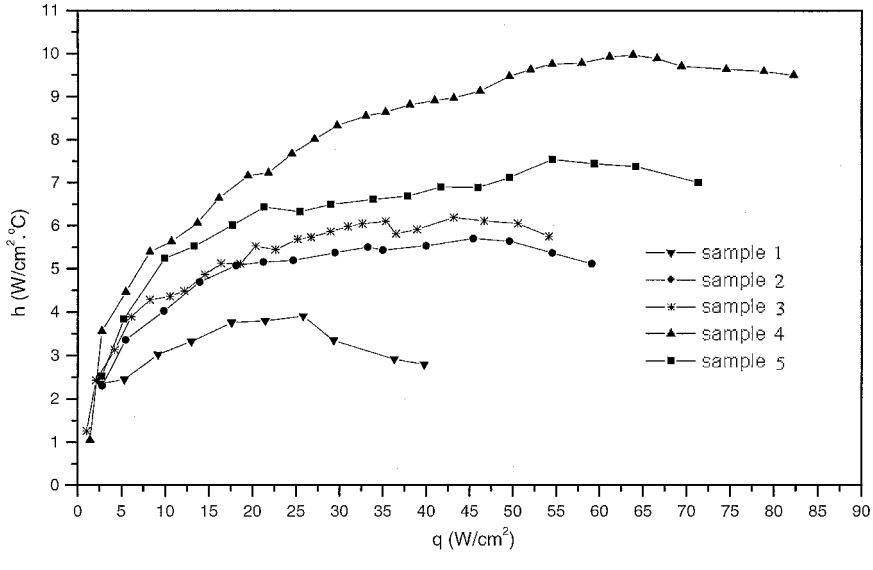

Fig. 4 Heat transfer coefficient vs imposed heat flux at $\Delta H = 4.0$ mm.

We now turn our attention to the comparison of heat transfer coefficient between the monodispersed wicks and the bidispersed wicks, as shown in Fig. 4. We first compare sample 1 (a monodispersed wick having a pore diameter of 80 μm) and sample 3 (a bidispersed wick having a pore-diameter ratio of 200/80 μm). As can be seen from Fig. 4, the bidispersed wick having a large/small pore-diameter ratio of 200/80 μm (sample 3) has a higher heat transfer coefficient and critical heat flux than that of the monodispersed wick having a pore diameter of 80 μm (sample 1). The primary reason leading to the improvement of the heat transfer performance by using the bidispersed wick was because its large pores provided a low flow resistance for vapor to escape, even though the capillary forces provided by both wicks were similar because the small-pore diameter of the bidispersed wick had the same value as the pore diameter of the monodispersed wick. We now compare the performance of the monodispersed wick having a pore diameter of 800 μm (sample 2) and those of the bidispersed wick having a pore-diameter ratio of 800/80 μm (sample 5) in Fig. 4. It is seen from Fig. 4 that sample 5 exhibits higher heat transfer coefficients and a higher critical heat flux than sample 2. The improvement was primarily because the capillary force generated in the small pores (80 μm) of the bidispersed wick is much larger than that generated by the monodispersed wick having large pores (800 μm), although there is not much difference in the flow resistance of both wicks.

We now examine the influence of the large-pore diameters on the heat transfer performance of bidispersed wicks (samples 3–5) having the same small diameter of 80 μm. It is seen from Fig. 4 that among these three bidispersed wicks, sample 4 (with a pore-diameter ratio of 400/80 μm) exhibits both the highest heat transfer coefficient and the highest critical heat flux. This implies that there exists an optimal large-pore diameter for a given small-pore diameter. This can be explained as follows: For a fixed size of small pores, an increase of the large-pore diameters, on the one hand, will lead to an increase in the effective permeability of the bidispersed wick, resulting in a low flow resistance for vapor to escape to the vapor grooves. This helps to increase the mass flow rate of the subcooled liquid and, thus, may lead to the increase of both the heat transfer coefficient and the critical heat flux (comparing samples 3 and 5). On the other hand, an increase of the large-pore diameter causes a reduction in the capillary force in the macropores. This effect causes a decrease in the mass flow rate of the subcooled liquid, leading to a decrease in both the heat transfer coefficient and the critical heat flux (comparing samples 4 and 5). Therefore, for bidispersed wicks having a fixed small-pore diameter, there exists an optimal large-pore

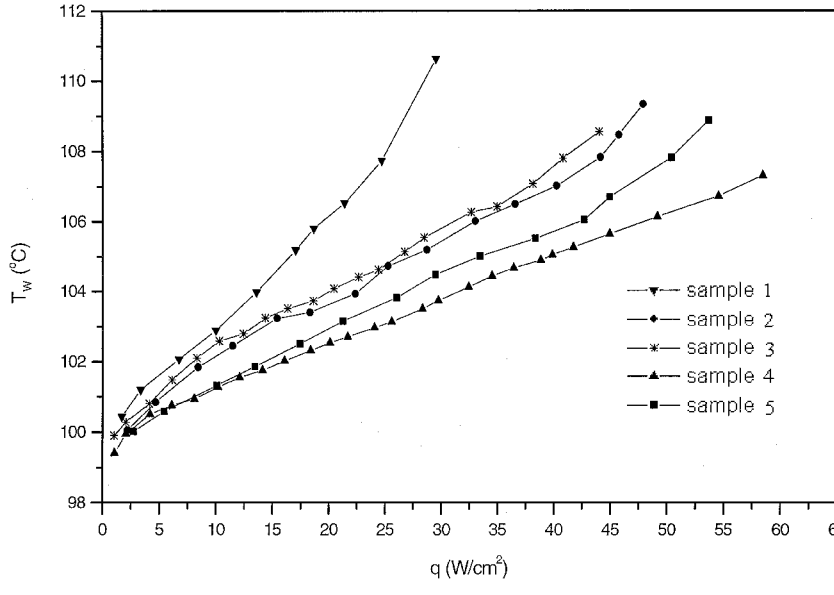

Fig. 5 Mean temperature of the heating block vs imposed heat flux at $\Delta H = 7.0$ mm.

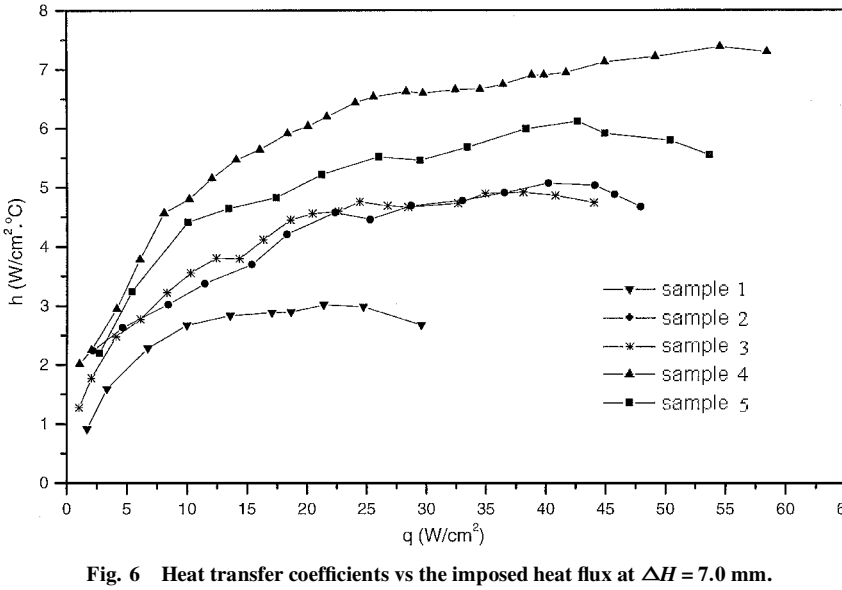

Fig. 6 Heat transfer coefficients vs the imposed heat flux at $\Delta H = 7.0$ mm.

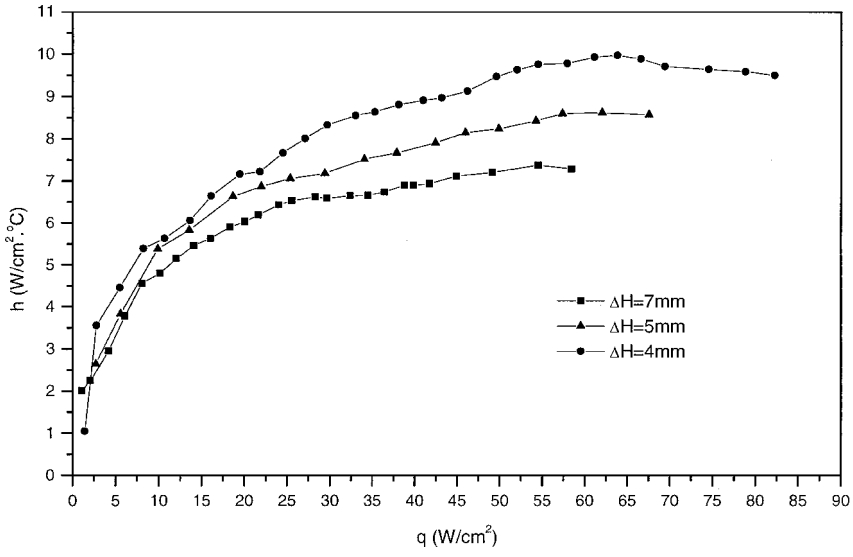

Fig. 7 Effects of the adverse hydrostatic head on the heat transfer performance for sample 4.

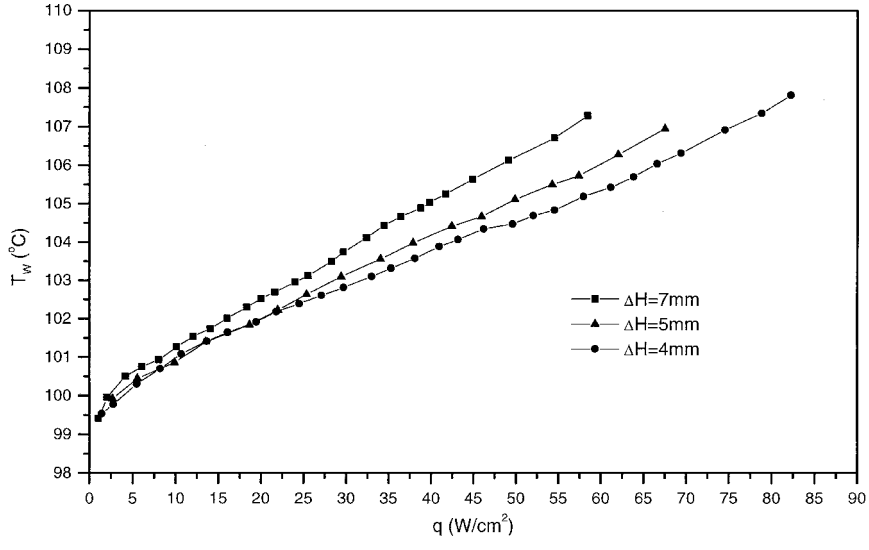

Fig. 8 Effects of the adverse hydrostatic head on the mean temperature of the heating block for sample 4.

diameter that gives both the highest heat transfer coefficient and the highest critical heat flux. Also note from Fig. 3 that sample 4 gives the lowest heating block mean temperatures among the three bidispersed porous samples.

Figures 5 and 6 show similar variations of the mean temperature of the heating block and the heat transfer coefficient vs the imposed heat flux at $\Delta H = 7.0$ mm. A comparison of Figs. 4 and 6 shows that when the adverse hydrostatic head was increased from 4.0 to 7.0 mm, both the heat transfer coefficient and the critical heat flux generally decreased. The mean temperature of the heating block for $\Delta H = 7.0$ mm presented in Fig. 5 is higher than that presented in Fig. 3 for $\Delta H = 4.0$ mm.

To further examine the effect of the adverse hydrostatic head ($\Delta H = 4.0$, 5.0, and 7.0 mm) on the heat transfer performance, the variation of the heat transfer coefficient with the imposed heat flux for the bidispersed wick of sample 4 is presented in Fig. 7. It is clear from Fig. 7 that both the transfer coefficient and the critical heat flux increase with the decrease of the adverse hydrostatic head. This can be explained as follows: In the present problem, the capillary force is the driving force that must overcome the adverse hydraulic and the drag force to push the liquid rising up to the heated surface. For a smaller adverse hydrostatic head, the net capillary force becomes relatively larger, and, therefore, a larger amount of liquid can be supplied to the upper layer. As a result, both the heat transfer coefficient and critical heat flux increase with a decrease of the adverse hydrostatic head. For the same reason, as shown in Fig. 8, the mean temperature of the heating block decreases with a decrease of the adverse hydrostatic head.

Conclusions

In this paper, we have presented the experimental results on evaporative heat transfer characteristics of sintered copper bidispersed wicks heated by a grooved block at the top. The experimental results show that, when a monodispersed wick is replaced by a bidispersed wick whose small-pore diameter is the same as that of a monodispersed wick, both the heat transfer coefficient and critical heat flux are increased substantially. For bidispersed wicks having the same small-pore diameter, there exists an optimal large-pore diameter that gives both the highest heat transfer coefficient and the highest critical heat flux. It is also found that heat transfer performance of bidispersed wicks is improved as the adverse hydrostatic head is reduced.

Acknowledgments

This work was supported by Hong Kong Research Grants Council Earmarked Research Grants HKUST6044/97E, HKUST 6178/00E, and HIA98/99.EG04.

References

[1]Fredley, J., and Pelszynke, A., "Accommodation of the EOS AM Instrument Set Using Capillary Pumped Heat Transport Technology," Society of Automotive Engineers, SAE Paper 921404, 1992.

[2]Clayton, S., Martin, D., and Bauman, J., "Mars Surveyor Thermal Management Using a Fixed Conductance Capillary Pumped Loop," *SAE Transactions*, Vol. 106, No. 1, 1997, pp. 899–910.

[3]Deng, Q., Ma, T., Zhang, Z., and Wang, J., "Experimental Investigation on the Performance of Evaporator for Capillary Pumped Loops," *Journal of Engineering Thermophysics*, Vol. 19, No. 3, 1998, pp. 330–334.

[4]Cao, Y. D., and Faghri, A., "Analytical Solutions of Flow and Heat Transfer in a Porous Structure with Partial Heating and Evaporation on the Upper Surface," *International Journal of Heat and Mass Transfer*, Vol. 37, No. 10, 1994, pp. 1525–1533.

[5]Cao, Y. D., and Faghri, A., "Conjugate Analysis of a Flat-Plate Type Evaporator for Capillary Pumped Loops with 3-Dimensional Vapor Flow in the Groove," *International Journal of Heat and Mass Transfer*, Vol. 37, No. 3, 1994, pp. 401–409.

[6]Khrustalev, D., and Faghri, A., "Heat Transfer in the Inverted Meniscus Type Evaporator at High Heat Fluxes," *International Journal of Heat and Mass Transfer*, Vol. 38, No. 16, 1995, pp. 3091–3101.

[7]Liao, Q., and Zhao, T. S., "Evaporative Heat Transfer in a Capillary Structure Heated by a Grooved Block," *Journal of Thermophysics and Heat Transfer*, Vol. 13, No. 1, 1999, pp. 126–133.

[8]Zhao, T. S., and Liao, Q., "On Capillary-Driven Flow and Phase-Change Heat Transfer in a Porous Structure Heated by a Finned Surface: Measurements and Modeling," *International Journal of Heat and Mass Transfer*, Vol. 43, No. 7, 2000, pp. 1141–1155.

[9]Liao, Q., and Zhao, T. S., "A Visual Study of Phase-Change Heat Transfer in a Two-Dimensional Porous Structure with a Partial Heating Boundary," *International Journal of Heat and Mass Transfer*, Vol. 43, No. 7, 2000, pp. 1089–1102.

[10]Eastman, G. Y., Ernst, D. M., Shaubach, R. M., and Toth, J. E., "Advanced Heat Pipe Technology for Space Heat Transport and Rejection Technologies," *Space Power*, Vol. 9, No. 1, 1990, pp. 15–26.

[11]Vityaz, P. A., Konev, S. V., Medvedev, V. B., and Sheleg, V. K., "Heat Pipe with Bidispersed Capillary Structures," *Proceedings of the 5th International Heat Pipe Conference*, Japan Technology and Economics, Tokyo, Japan, 1984, pp. 127–135.

[12]Demidov, A. S., and Yatsenko, E. S., "Investigation of Heat and Mass Transfer in the Evaporation Zone of a Heat Pipe Operating by the 'Inverted Meniscus' Principle," *International Journal of Heat and Mass Transfer*, Vol. 37, No. 14, 1994, pp. 2155–2163.

[13]Ku, J., "Recent Advances in Capillary Pumped Loop Technology," AIAA Paper 97-3870, 1997, pp. 1–21.

[14]North, M. T., Rosenfeld, J. H., and Shaubach, R. M., "Liquid Film Evaporation from Bidisperse Capillary Wicks in Heat Pipe Evaporators," *Proceedings of the IX International Heat Pipe Conference*, Los Alamos National Lab., La-UR-97-1500, Los Alamos, NM, 1997, pp. 143–147.

[15]Chen, Z. Q., Cheng, P., and Zhao, T. S., "An Experimental Study of Two-Phase Flow and Boiling Heat Transfer in Bi-Dispersed Porous Channels," *International Communications in Heat and Mass Transfer*, Vol. 27, No. 3, 2001, pp. 293–302.

[16]Kline, S. J., and McClintock, F. A., "Describing Uncertainties in Single-Sample Experiments," *Mechanical Engineering*, Vol. 75, Jan. 1953, pp. 3–12.